Theoretical investigation of three-dimensional quasi-phase-matching photonic structures

Tamara Pogosian

Laboratoire de Photonique Quantique et Moléculaire, UMR 8537, Ecole Normale Supérieure de Cachan, CentraleSupelec, CNRS, Université Paris-Saclay, 61 avenue du Président Wilson, 94235 Cachan, France
and International laboratory "Nonlinear optical molecular crystals and microlasers," ITMO University, Kronverkskiy pr.49, 197101, Saint Petersburg, Russia

Ngoc Diep Lai[*]

Laboratoire de Photonique Quantique et Moléculaire, UMR 8537, Ecole Normale Supérieure de Cachan, CentraleSupelec, CNRS, Université Paris-Saclay, 61 avenue du Président Wilson, 94235 Cachan, France

We present a full theoretical analysis of quasi-phase-matching (QPM) in three-dimensional (3D) periodic structures and point up optimum nonlinear structures, which promote the best nonlinear conversion efficiencies and are close to real structures. The QPM properties of 14 Bravais lattices are investigated as a function of motifs (orthorhombic and spherical) and of modulation types ("+/−" and "+/0"). This full 3D QPM theory allows us to produce all results of one- and two-dimensional QPM structures by choosing appropriate lattice periodicity and motif. The optimization of nonlinear conversion efficiencies in 3D QPM is obtained by analyzing four particular structures (simple cubic, body-centered cubic, face-centered cubic, and diamond cubic lattices) with different filling factors and motifs. In particular, 3D structures, which are very close to those realized in practice, are proposed and simulated, creating a guide for fabrication of real optimum QPM structures.

I. INTRODUCTION

Nonlinear optics revealed a possibility to transform the fundamental property of light beams (its frequency), but it faced a problem of chromatic dispersion, which leads to phase mismatching and destructive interference with new light generated in different regions of the nonlinear material. Two main ways were proposed to compensate for this inherent lack of phase matching. Relying on birefringence of nonlinear medium by choosing correct "cut" or crystal orientation, birefringent crystals have been used for minimizing the phase mismatching of frequency conversion since the early 1960s [1,2]. However, this method showed an insuperable drawback of the given material properties, the dispersion and the birefringence, and hence not all phase-matching conditions can be satisfied due to the lack of proper crystal orientation. Besides, most birefringent crystals have a limitation of efficient length due to the "walk-off" effect [3–5].

Another solution, called quasi-phase-matching (QPM), was proposed independently in the 1960s [6,7] and it has been intensively developed since the mid-1990s. QPM is based on spatial modulation of nonlinear susceptibility to compensate for the phase mismatching between interacting waves. For efficient harmonic generation the modulation periodicity should be equal to twice the coherent length, which is in the range of micrometers. This method overcomes drawbacks of birefringent crystals: It can be applied to any nonlinear material and compensates for phase mismatching of any nonlinear process. Furthermore, it reveals simultaneous and multicascade complicated processes, as well as a new nonlinear optics effect, that cannot be realized with standard birefringent materials. The original ideal was proposed to modulate the nonlinear susceptibility in one dimension (1D) and the full theory is well presented in Ref. [8]. Many experimental works have been reported in agreement with the theory, demonstrating great advantages of the QPM technique comparing to the birefringence-based method. However, by using a periodic 1D QPM structure, applications are limited to a single wavelength and to a single nonlinear optics effect, such as second-harmonic generation (SHG). In 1998, Berger [9] released a study of QPM into 2D space. Two-dimensional periodical and quasiperiodical nonlinear structures provide plentiful reciprocal vectors used for noncollinear SHG [10], for simultaneous wavelength interchange [11], for third- and fourth-harmonic generations [12,13], for all-optical deflections and splitting [14], for optical parameter oscillation [15], and for various beam shaping [16–18]. Theoretically speaking, 3D QPM structures should be thoroughly studied in fundamental physics as well as potential applications. Compared to the 1D and 2D cases, 3D QPM structures provide more reciprocal lattice vectors to compensate the phase mismatches in more complicated nonlinear optical processes. However, only a few articles concerning 3D QPM have been reported [19,20], mainly due to the lack of fabrication technologies. Full understanding of 3D QPM and optimal 3D structures is therefore still missing.

For realization of QPM structures, various techniques have been suggested and applied for different kinds of nonlinear materials. An electric poling method has been used successfully to pole various ferroelectric crystals for 1D [21] and 2D [10] structures. Unfortunately, this poling technique seems to be almost impossible when used for obtaining 3D ferroelectric crystals, or it requires a fabrication process containing multiple complicated steps. Recently, it was found that naturally grown crystal can support broadband SHG [22], but randomness of 3D domains reduces frequency of conversion and this technique does not allow us to control the process to create

---

[*]nlai@lpqm.ens-cachan.fr

exact structures. Another fabrication technique is based on orientation pattering of semiconductors such as GaAs [23], and provides large nonlinearity and extensive transparency, but it is also not applicable in creating 3D QPM structures. The most promising materials for modulating the nonlinear coefficient in 3D are polymers. Numerous methods can be applied to realize 1D and 2D structures in polymers such as periodic poling [24], photothermal poling [25], all-optical poling [26], photodepoling with photolithographic masks [27], UV photo bleaching [28], two-beam interference [29], and direct laser writing [30,31]. As for 3D QPM structures, a few attempts of fabrication based on direct laser writing method with Disperse Red 1 (DR1) sol-gel polymer [32] and DR1-Poly-methyl-methacrylate copolymer [33] have been reported.

Theoretically speaking, second-order nonlinear susceptibility, $\chi^{(2)}$, is periodically modulated by reversing the sign of domains with a periodicity determined by the coherence length of the nonlinear crystal. The best QPM structure is obtained by reversing the domain by 180° with a ratio of 50-50 between two domains (called "+" and "−") and with a periodicity of 2 times the coherence length [8]. The "+/−" QPM 1D and 2D structures have been fabricated in ferroelectrics [10,21,22], semiconductors [23], and polymers [24–26,28]. Another possibility to demonstrate the QPM effect is to modulate the nonlinear material [$\chi^{(2)} \neq 0$] with a linear material, which possesses a $\chi^{(2)}$ null. This QPM structure is named "+/0," which is less efficient than the "+/−" QPM structure but it is very easy to implement in experiment, in particular in the case of polymer materials [27,29–31]. This type of QPM structure ("+/0") may be unique to realize 3D QPM structures.

Indeed, the "+/0" QPM structures could be realized by using nonlinear polymer materials and the interference technique. The interference technique allows us to realize very large and uniform 1D, 2D, and 3D polymeric structures ($\chi^{(2)} = 0$), with filling factor and periodicity kept under control [34]. By filling the air holes of the fabricated structures with a nonlinear polymer material, we can obtain a desired "+/0" QPM structure. This technique is probably unique to realize 3D QPM structures. It is therefore necessary to investigate in detail the theory of 3D QPM method and to find out optimum 3D structures.

It seems to have a connection with so-called photonic crystal or nonlinear photonic crystal. However, it should borne in mind that the periodicity of QPM structure is twice the coherence length (micrometer range) while the periodicity of photonic crystal is less than half of the photonic bandgap wavelength (submicrometer range). Moreover, the QPM structures also requires a large filling factor of the nonlinear material in order to achieve a high nonlinear conversion efficiency. This requires a full understanding of 3D QPM structures for optimizing experimental implementation.

This paper is organized as follows: In the second section, we begin with a general theory of 3D QPM structures and establish a relation of nonlinear conversion efficiency with 3D lattices type and its motif. We will show that this general theory can be applied in order to obtain the results reported in Ref. [8] for 1D QPM structures and in Ref. [35] for 2D ones. The third section is devoted to the influence of structure motif in the case of 3D QPM. We investigate two

kinds of motifs in particular, orthorhombic and spherical, and determine nonlinear conversion efficiency for different 3D QPM orders and also compare new results with those obtained in 1D and 2D QPM structures reported in previous papers. In Sec. IV we present an optimization of QPM 3D structures, which also includes connection with practical structures. In the last section, we summarize the theoretical results and announce further work concerning experimental demonstration of 3D QPM structures.

II. GENERAL THEORY OF 3D QPM STRUCTURES

A. Wave equations in 3D QPM structures

This paper focuses on collinear SHG, but results can be easily applicable to other three-wave mixing processes. Concerning electric field and coupled-wave equations for 3D QPM structures, we adapted the generalization from Ref. [36]. The electric field in the QPM structure for the second harmonic (SH) with a new frequency 2ω can be written as

$$\widetilde{E}_{2\omega}(\mathbf{r},t) = \tfrac{1}{2} E_{2\omega}(\mathbf{r}) \exp[i(2\omega t - \mathbf{k}_{2\omega} \cdot \mathbf{r})] + \text{c.c.}, \quad (1)$$

where $\mathbf{r} \equiv (x,y,z)$ is the 3D spatial coordinates. Using slowly varying amplitude approximation, $\nabla^2 E_{2\omega}(\mathbf{r}) \ll \mathbf{k}_{2\omega} \nabla E_{2\omega}(\mathbf{r})$, and assuming that the amplitude of the fundamental wave is constant throughout the entire interaction length, the evolution of the SH field amplitude can be written as:

$$\mathbf{k}_{2\omega} \nabla E_{2\omega}(\mathbf{r}) = -2i \frac{\omega^2}{c^2} E_\omega^2 d(\mathbf{r}) \exp[i(\mathbf{k}_{2\omega} - 2\mathbf{k}_\omega)\mathbf{r}], \quad (2)$$

where $d(\mathbf{r}) = \chi_{ijk}^{(2)} \cdot g(\mathbf{r})/2$ is a nonlinearity function and $g(\mathbf{r})$ is a normalized and dimensionless function, representing space dependence of the nonlinear coefficient function. In QPM structures, it can be presented as a Fourier series,

$$g(\mathbf{r}) = \sum \mathbf{G}_{mnq} \cdot \exp(i\mathbf{K}_{mnq} \cdot \mathbf{r}), \quad (3)$$

where the sum is extended over the whole 3D reciprocal lattice (RL), $\mathbf{G}_{mnq}$ are Fourier coefficients, and $\mathbf{K}_{mnq}$ are RL vectors (RLVs), which depend on orders m, n, and q. $\mathbf{k}_{2\omega} - 2\mathbf{k}_\omega = \Delta\mathbf{k}$ is a mismatching vector between wave vectors of SH and fundamental waves. It can be compensated by one of the grating vectors $\mathbf{K}_{mnq}$. To find out the electric field, and hence intensity, we can directly integrate Eq. (2) using numerical methods. It can be applied to any periodic or aperiodic structure. In this study it is convenient to use the Fourier transform approach [8,35] to understand the influence of motif and lattice on SHG efficiency and to optimize final configuration.

As for the 3D QPM structure it can be modeled as a convolution of a periodic lattice and a nonlinear motif with function $s(\mathbf{r})$ (Fig. 1). A motif represents, for example, a $\chi^{(2)}$ with a positive sign, "+1", while other surrounding material possesses a $\chi^{(2)}$ with a negative sign "−1" or a null value ("0"). If we assume that (m,n,q)-order satisfies the phase matching condition, i.e., $\Delta\mathbf{k} - \mathbf{K}_{mnq} = 0$, while all other orders contribute negligible oscillating terms, after an interaction length, L, SH intensity can be calculated as

$$I_{2\omega} \approx \frac{2\omega^2 \chi_{ijk}^{(2)} |\mathbf{G}_{mnq}|^2}{n_{2\omega} n_\omega^2 c^3 \varepsilon_0} I_\omega^2 L^2, \quad (4)$$
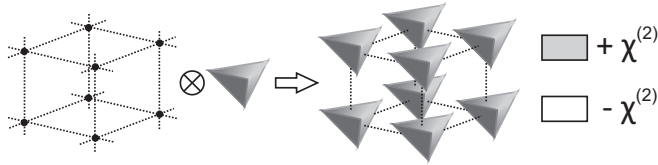
FIG. 1. Convolution of a simple cubic lattice with a triangular motif to model 3D periodic QPM structure.

with

$$\mathbf{G}_{mnq} = \frac{1}{V} \int s(\mathbf{r}) \exp(i\mathbf{K}_{mnq} \cdot \mathbf{r}) d^3\mathbf{r}$$
$$= \frac{1}{V} S(\mathbf{K}_{mnq}/2\pi), \quad (5)$$

where the integration is taken over repeating unit cell, V is a unit cell volume, and $S(\mathbf{f})$ is Fourier transform of the motif. It is clear that Fourier coefficient depends on type of lattice, $\mathbf{K}_{mnq}$, and type of motif, $s(\mathbf{r})$.

B. 3D QPM structures: Real and reciprocal lattices

Mathematically, periodical QPM structure can be treated by the same way as a regular periodical crystal, which is well described in Ref. [37]. In 3D space, there are 14 types of Bravais lattice, grouped into seven lattice systems: triclinic, monoclinic, orthorhombic, tetragonal, cubic, trigonal, and hexagonal.

Each 3D lattice is defined by three fundamental translation vectors, $\mathbf{a}_1$, $\mathbf{a}_2$, and $\mathbf{a}_3$. Hence all real lattice points $\mathbf{r}$ are determined by a set of arbitrary integers u_1, u_2, and u_3,

$$\mathbf{r} = u_1 \mathbf{a}_1 + u_2 \mathbf{a}_2 + u_3 \mathbf{a}_3. \quad (6)$$

The primitive vectors $\mathbf{a}_1$, $\mathbf{a}_2$, and $\mathbf{a}_3$ are described by lengths a, b, and c, respectively, and by three angles α, β, and γ (see Fig. 2) and can be represented as:

$$\mathbf{a}_1 = a(1,0,0), \quad (7a)$$

$$\mathbf{a}_2 = b(\cos\gamma, \sin\gamma, 0), \quad (7b)$$

$$\mathbf{a}_3 = c(\cos\beta, \cos\alpha\sin\gamma, \sin\alpha\sin\beta). \quad (7c)$$

Here $\mathbf{a}_1$ belongs to the x axis, $\mathbf{a}_2$ lies in the xy plane, and $\mathbf{a}_3$ is determined by all three axes. Volume of the unit cell can be calculated as $V = abc \sin\alpha \sin\beta \sin\gamma$.
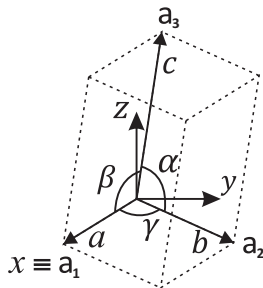
FIG. 2. Illustration of a triclinic unit cell, with different parameters defined in the text.

Similarly to a regular periodical crystal, RLVs can be found in the relation $\mathbf{a}_i \cdot \mathbf{b}_j = 2\pi\delta_{ij}$. Hence, in the general case, RLVs are determined by

$$\mathbf{b}_1 = \frac{2\pi}{a}\left(1, \frac{-1}{\tan\gamma}, \left(\frac{\cos\gamma}{\tan\alpha\sin\beta} - \frac{1}{\tan\beta\sin\alpha}\right)\right), \quad (8a)$$

$$\mathbf{b}_2 = \frac{2\pi}{b}\left(0, \frac{1}{\sin\gamma}, \frac{-1}{\tan\alpha\sin\beta}\right), \quad (8b)$$

$$\mathbf{b}_3 = \frac{2\pi}{c}\left(0, 0, \frac{1}{\sin\alpha\sin\beta}\right). \quad (8c)$$

The 3D reciprocal lattice points are given by

$$\mathbf{K}_{mnq} = m\mathbf{b}_1 + n\mathbf{b}_2 + q\mathbf{b}_3. \quad (9)$$

Table I presents parameters, primitive vectors, unit cell volume, and RLVs of four particular 3D lattices.

III. INFLUENCE OF STRUCTURE MOTIF

In this section we discuss the influence of structures motifs on the nonlinear coefficients. By varying parameters of the motif for each QPM, an order-relevant Fourier coefficient can be found. This ensures investigating efficiency for a given structure as a function of dimensions and shape of the motif. We can determine the highest efficiency or completely null of conversion efficiency, which is useful for nullifying unwanted processes.

A. Orthorhombic motif

The orthorhombic motif is defined by:

$$s(\mathbf{r}) = \text{rect}\left(\frac{x}{X}\right)\text{rect}\left(\frac{y}{Y}\right)\text{rect}\left(\frac{z}{Z}\right), \quad (10a)$$

where

$$\text{rect}(u) = \begin{cases} +1 & |u| \leqslant \frac{1}{2} \\ p & \text{elsewhere} \end{cases}. \quad (10b)$$

Here p is equal -1 for "$+/-$" QPM structures and p is equal 0 for "$+/0$" QPM structures. The corresponding Fourier transform is calculated by:

$$S(\mathbf{f}) = P(XYZ)[\text{sinc}(f_x X)\text{sinc}(f_y Y)\text{sinc}(f_z Z)] \quad (11)$$

where the "sinc" function is defined as $\text{sinc}(x) = \sin(x)/x$; X, Y, and Z are the sizes of an orthorhombic motif in three dimensions; $P = 2$ for "$+/-$" QPM structures; and $P = 1$ for "$+/0$" QPM structures. Table II(a) displays the Fourier coefficients of four types of lattices made by an orthorhombic motif. These coefficients are calculated for "$+/-$" structures, which are twice as large as nonlinear coefficients for "$+/0$" QPM structures. Obviously, it is hard to illustrate all possible coefficients for each QPM order due to a number of variables; however, we can distinguish most efficient parameters using knowledge of the "sinc" function. We should remember that motifs should not overlap with each other, otherwise the Fourier transform approach will not provide the correct result. Hence, in the case of orthorhombic and square lattices, the size of the motif should not exceed the size of a unit cell, i.e., $X/a \leqslant 1$.

Using this general theory, we can calculate the nonlinear coefficients of any 1D, 2D, and 3D structures and find out

TABLE I. Parameters, primitive vectors, unit cell volume, and RLVs of four particular 3D lattices

	Triclinic	Orthorhombic	Cubic	Hexagonal
Parameters	$a \neq b \neq c$ $\alpha \neq \beta \neq \gamma$	$a \neq b \neq c$ $\alpha = \beta = \gamma = 90°$	$a = b = c$ $\alpha = \beta = \gamma = 90°$	$a = b \neq c$ $\alpha = \beta = 90°, \gamma = 120°$
Primitive vectors	$\mathbf{a}_1 = a(1,0,0)$ $\mathbf{a}_2 = b(\cos \gamma, \sin \gamma, 0)$ $\mathbf{a}_3 = c(\cos \beta, \cos \alpha \sin \gamma, \sin \alpha \sin \beta)$	$\mathbf{a}_1 = a(1,0,0)$ $\mathbf{a}_2 = b(0,1,0)$ $\mathbf{a}_3 = c(0,0,1)$	$\mathbf{a}_1 = a(1,0,0)$ $\mathbf{a}_2 = a(0,1,0)$ $\mathbf{a}_3 = a(0,0,1)$	$\mathbf{a}_1 = a(1,0,0)$ $\mathbf{a}_2 = a(-\frac{1}{2},\frac{\sqrt{3}}{2},0)$ $\mathbf{a}_3 = c(0,0,1)$
Unit cell volume	$V = abc \sin \alpha \sin \beta \sin \gamma$	$V = abc$	$V = a^3$	$V = a^2 c \frac{\sqrt{3}}{2}$
RLVs	$\mathbf{b}_1 = \frac{2\pi}{a}(1, \frac{-1}{\tan \gamma}, (\frac{\cos \gamma}{\tan \alpha \sin \beta} - \frac{1}{\tan \beta \sin \alpha}))$ $\mathbf{b}_2 = \frac{2\pi}{b}(0, \frac{1}{\sin \gamma}, \frac{-1}{\tan \alpha \sin \beta})$ $\mathbf{b}_3 = \frac{2\pi}{c}(0,0,\frac{1}{\sin \alpha \sin \beta})$	$\mathbf{b}_1 = \frac{2\pi}{a}(1,0,0)$ $\mathbf{b}_2 = \frac{2\pi}{b}(0,1,0)$ $\mathbf{b}_3 = \frac{2\pi}{c}(0,0,1)$	$\mathbf{b}_1 = \frac{2\pi}{a}(1,0,0)$ $\mathbf{b}_2 = \frac{2\pi}{a}(0,1,0)$ $\mathbf{b}_3 = \frac{2\pi}{a}(0,0,1)$	$\mathbf{b}_1 = \frac{2\pi}{a}(1,\frac{1}{\sqrt{3}},0)$ $\mathbf{b}_2 = \frac{2\pi}{a}(0,\frac{2}{\sqrt{3}},0)$ $\mathbf{b}_3 = \frac{2\pi}{c}(0,0,1)$

the optimum QPM structures. Indeed, choosing the first-order $(m,n,q) = (1,0,0)$, we obtained a 1D QPM structure. The highest nonlinear coefficient, $|\mathbf{G}_{100}|^2 = 0.405$, was obtained with the following parameters: $X/a = 0.5$, $Y/b = 1$, and $Z/c = 1$, which is very consistent with the results published in Ref. [36]. We called it a 1D-like structure, and it is presented in Fig. 3(a). Similarly, by using the second QPM order $(1,1,0)$ relying on two primitive vectors, we obtained a 2D QPM structure, as shown in Fig. 3(b), with the highest nonlinear coefficient $|\mathbf{G}_{110}|^2 = 0.041$. The new QPM order $(1,1,1)$, which appears in 3D structures, relies on all three primitive vectors. It has a value $|\mathbf{G}_{111}|^2 = 0.004$ with parameters $X/a = 0.5$, $Y/b = 0.5$, and $Z/c = 0.5$ [Fig. 3(c)].

Note that for 3D QPM the nonlinear coefficient depends on many parameters, for example, the propagation direction of the fundamental light beam through the nonlinear crystal. For the following analysis, we can fix the 3D structure as shown in Fig. 3(c), and calculate the nonlinear efficiency for different orders. For the first order $(m,n,q) = (1,0,0)$, we obtained $|\mathbf{G}_{100}|^2 = 0.025$, which is 16 times smaller than that of the 1D-like structure shown in Fig. 3(a). This is explained by the fact that in a 3D QPM structure there is 4 times less working material comparing to a 1D-like structure, resulting in a 4×4 times weaker nonlinear coefficient. A similar thing occurs with order $(m,n,q) = (1,1,0)$: We obtained $|\mathbf{G}_{110}|^2 = 0.010$ and it

is 4 times smaller than that of the 2D-like structure [shown in Fig. 3(b)], due to 2 times less working material.

B. Spherical and cylindrical motif

Spherical motif ($\chi^{(2)} = +1$) with radius R immersed in a background of [$\chi^{(2)} = -1$ or 0] is determined as:

$$s(\mathbf{r}) \equiv \begin{cases} +1 & |\mathbf{r}| \leqslant R \\ p & \text{elsewhere.} \end{cases} \quad (12)$$

Here p is equal -1 for "$+/-$" QPM structures and p is equal 0 for "$+/0$" QPM structures. Corresponding Fourier transform is calculated by:

$$S(\mathbf{f}) = \frac{4\pi P}{|\mathbf{f}^3|}[\sin(|\mathbf{f}|R) - |\mathbf{f}|R \cos(|\mathbf{f}|R)], \quad (13)$$

where $P = 2$ for "$+/-$" QPM structures and $P = 1$ for "$+/0$" QPM structures.

Table II(b) displays the Fourier coefficients of a spherical motif for four types of lattice. The normalized efficiency for 3D lattice can be analyzed as a function of ratio between spherical radius and length of primitive vector. The ratio R/a should not exceed 0.5. In orthorhombic lattice, normalized efficiency can be examined by the function $\mathbf{G}_{mnq}(R/a; a/b; a/c)$, where a is the length of the shortest primitive vector, hence $R/a \leqslant 0.5$,

TABLE II. Fourier coefficient of (a) an orthorhombic motif and (b) a spherical motif for "$+/-$" QPM structures

Lattice type	Fourier coefficients
(a) Fourier coefficient of an orthorhombic motif	
Triclinic	$\mathbf{G}_{mnq} = \frac{2XYZ\,\text{sinc}(m\frac{X}{a})\text{sinc}(Y\frac{an-bm\cos\gamma}{ab\sin\gamma})\text{sinc}(Z\frac{abq-acn\cos\alpha+cbm(\cos\alpha\cos\gamma-\cos\beta)}{abc\sin\alpha\sin\beta})}{abc\sin\alpha\sin\beta\sin\gamma}$
Orthorhombic	$\mathbf{G}_{mnq} = 2\frac{XYZ}{abc}\text{sinc}(m\frac{X}{a})\text{sinc}(n\frac{Y}{b})\text{sinc}(q\frac{Z}{c})$
Square	$\mathbf{G}_{mnq} = 2\frac{XYZ}{a^3}\text{sinc}(m\frac{X}{a})\text{sinc}(n\frac{Y}{a})\text{sinc}(q\frac{Z}{a})$
Hexagonal	$\mathbf{G}_{mnq} = 2\frac{XYZ}{a^2c\sqrt{3}}\text{sinc}(m\frac{X}{a})\text{sinc}((m+2n)\frac{Y}{a\sqrt{3}})\text{sinc}(q\frac{Z}{c})$
(b) Fourier coefficient of a spherical motif	
	$\mathbf{G}_{mnq} = \frac{8\pi}{|\mathbf{K}|^3 V}(\sin(|\mathbf{K}|R) - |\mathbf{K}|R\cos(|\mathbf{K}|R))$
Triclinic	$|\mathbf{K}| = 2\pi\sqrt{\frac{m^2}{a^2} + \frac{(an-bm\cos\alpha)^2}{a^2b^2(\sin\gamma)^2} + \frac{(abq-acn\cos\alpha+cbm(\cos\alpha\cos\gamma-\cos\beta))^2}{a^2b^2c^2(\sin\alpha\sin\beta)^2}}$
Orthorhombic	$|\mathbf{K}| = 2\pi\sqrt{\frac{m^2}{a^2} + \frac{n^2}{b^2} + \frac{q^2}{c^2}}$
Square	$|\mathbf{K}| = \frac{2\pi}{a}\sqrt{m^2 + n^2 + q^2}$
Hexagonal	$|\mathbf{K}| = 2\pi\sqrt{\frac{4(m^2+mn+n^2)}{3a^2} + \frac{q^2}{c^2}}$
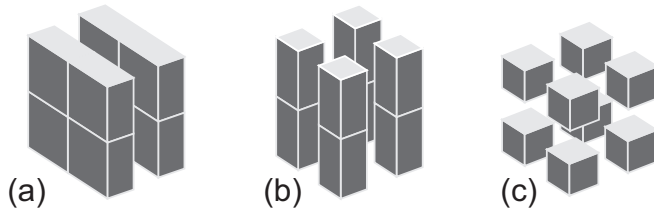
FIG. 3. (a) 1D-like structure with parameters $X/a = 0.5$, $Y/b = 1$, and $Z/c = 1$; (b) 2D-like structure with parameters $X/a = 0.5$, $Y/b = 0.5$, and $Z/c = 1$; (c) 3D structure with parameters $X/a = 0.5$, $Y/b = 0.5$, and $Z/c = 0.5$.

$a/b \leqslant 1$, and $a/c \leqslant 1$. It shows that the first QPM orders relying on different RLVs are not equal (see Fig. 4). For example, in orthorhombic lattice, first orders $(0, 1, 0)$ [Fig. 4(b)] or $(0, 0, 1)$ [Fig. 4(c)] provide significantly high efficiency ($|\mathbf{G}_{010}|^2 = 0.190$ with parameters $R/a = 0.5$, $a/b = 0.65$, and $a/c = 1$. These results are similar to those obtained with a rectangular lattice and circular motif reported in Ref. [38]. But when the fundamental light propagates along the shortest primitive vector, a maximum nonlinear coefficient of the first order, which we can achieve, is $|\mathbf{G}_{100}|^2 = 0.101$ with parameters $R/a = 0.5$, $a/b = 1$, and $a/c = 1$ [Fig. 4(a)]. Obviously, this value is the best for cubic lattice, where it has equivalent lattices for three dimensions.

Note that, unlike the orthorhombic motif shown in the previous section, while using a spherical motif, it is difficult to obtain equivalent 1D and 2D structures with an optimum nonlinear coefficient (see Fig. 5). We have already shown that the highest nonlinear coefficient for the rectangular motif in a rectangular lattice (2D) and the orthorhombic motif in an orthorhombic lattice (3D) is $|\mathbf{G}_{10}|^2 = |\mathbf{G}_{100}|^2 = 0.405$ and it is the same as that of a 1D structure. However, the highest normalized efficiency for a rectangular lattice with a circular motif is $|\mathbf{G}_{10}|^2 = 0.338$ with parameters $R/a_2 = 0.5$ and $R/a_1 = 0.29$ [38]. The highest normalized efficiency for the orthorhombic lattice with a spherical motif was mentioned above and is equal to $|\mathbf{G}_{010}|^2 = 0.190$. These data show that the most optimum structures with circular and spherical motifs are similar to that of a 1D periodic structure and they have quite high efficiency compared with other 2D and 3D structures but lower than the 1D QPM structure. But this high efficiency is
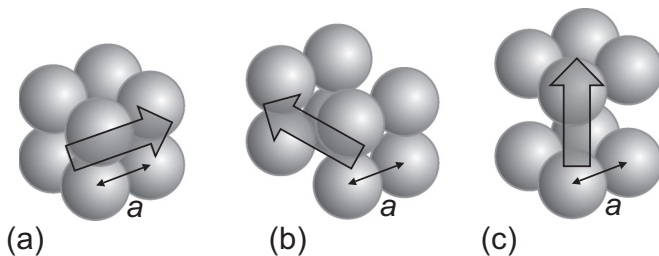
FIG. 4. Optimum configurations of a 3D QPM structure with orthorhombic lattice, spherical motif, and the shortest side a depending on QPM order: (a) $(1, 0, 0)$ order for collinear QPM means that fundamental light propagates along the shortest side of the lattice, (b) $(0, 1, 0)$ order, and (c) $(0, 0, 1)$ order both have propagation of fundamental light perpendicular to the shortest side.
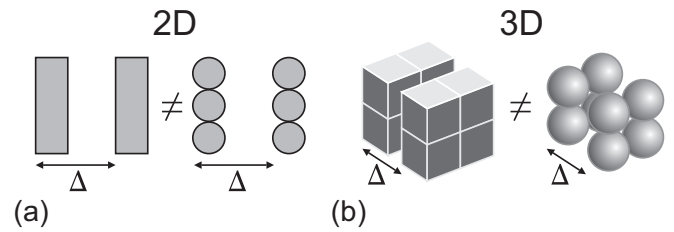
FIG. 5. Schematic comparison of QPM structures with (a) rectangular and circular motif in 2D and (b) orthorhombic and spherical motif in 3D.

useful only for phase matching a single process and this is the biggest drawback of these structures.

We concluded that the general theory proposed in this work could be applied to any 1D, 2D, and 3D QPM structures. But the optimum QPM structure depends largely on the chosen motif as well as on the type QPM lattice (see next section). Figure 6 shows, for example, extension of 2D structure to 3D space using cylindrical and spherical motif with different motif/periodic ratios. The 2D structure and the structure in Fig. 6(a) have the same efficiency of the first QPM order and it is higher than in other structures, but all other structures have more orders useful for QPM in all three dimensions. The spherical motif seems to be the only appropriate one for the formation of 3D QPM structures due to its symmetry. In the next section, we will focus on the optimization of 3D QPM structures by investigating the nonlinear coefficients as a function of spherical and cubic motifs, of the filling factor of the 3D QPM structures, and the propagation direction of the fundamental light beam.

IV. OPTIMIZATION OF QPM 3D STRUCTURES

In this section, we present research on optimum 3D QPM structures. First, we show the results of several particular 3D structures, which possess the highest nonlinear coefficients. Then, we show the results obtained with modified 3D QPM structures, in which the motifs are connected by small features that are very close to the real structures fabricated in practice.

A. Optimum 3D QPM structures

It is well known that in the case of photonic crystal, diamond cubic (DC) lattices possesses the best photonic bandgap [39]. However, it does not mean that the same situation is observed in
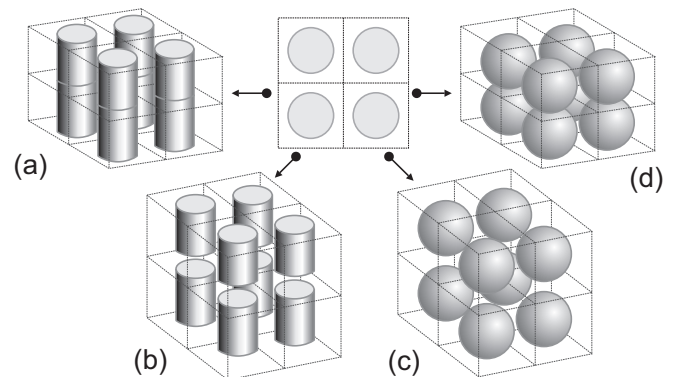
FIG. 6. Extension of 2D structure to 3D space using cylindrical and spherical motifs, with different motif/period ratios.

TABLE III. Fourier coefficients and limitations of motifs for SC, BCC, FCC, and DC lattices for "+/–" QPM structures.

Lattice types	Fourier coefficients
Simple cubic	For cubic motif: $\mathbf{G}_{sc} = 2\frac{X^3}{a^3}\text{sinc}(m\frac{X}{a})\text{sinc}(n\frac{X}{a})\text{sinc}(q\frac{X}{a})$, $\frac{X}{a} \leqslant 1$ For spherical motif: $H = 2\pi\sqrt{m^2 + n^2 + q^2}$ $\mathbf{G}_{sc} = \frac{8\pi}{H^3}[\sin(H\frac{R}{a}) - H\frac{R}{a}\cos(H\frac{R}{a})]$, $\frac{R}{a} \leqslant 0.5$
Body-centered cubic	$\mathbf{G}_{bcc} = \mathbf{G}_{sc}\{1 + \exp[i\pi(m+n+q)]\}$, $\frac{X}{a} \leqslant 0.5$, $\frac{R}{a} \leqslant \frac{\sqrt{3}}{4}$
Face-centered cubic	$\mathbf{G}_{fcc} = \mathbf{G}_{sc}\{1 + \exp[i\pi(n+q)] + \exp[i\pi(m+q)] + \exp[i\pi(m+n)]\}$, $\frac{X}{a} \leqslant 0.5$, $\frac{R}{a} \leqslant \frac{\sqrt{2}}{4}$
Diamond cubic	$\mathbf{G}_{dc} = \mathbf{G}_{fcc}\{1 + \exp[i\pi(m+n+q)/2]\}$, $\frac{X}{a} \leqslant 0.25$, $\frac{R}{a} \leqslant \frac{\sqrt{3}}{8}$

QPM structures for nonlinear processes. Indeed, as mentioned previously, in the case of nonlinear optics, it requires a balance between the high symmetry of the photonic structures and the nonlinear material quantity. By calculating all 14 Bravais lattices and a few varieties, we found that just some of them possess high nonlinear coefficients. We report here only some, namely, simple cubic (SC), body-centered cubic (BCC), face-centered cubic (FCC), and DC lattices, and compare their nonlinear coefficients. For all these structures, we used cubic and spherical motifs as the simplest symmetric motifs, which are also similar to real structures.

The simplest 3D structure is the SC structure [37]. The Fourier coefficients for three other lattices can be calculated easily with the help of the theory presented previously or using a method to describe complex periodic structures with more simple ones, where basis has two or more points. For example, the BCC lattice can be presented as two shifted SC lattices, the FCC lattice consists of four SC lattices, and the DC lattice is a set of two FCC lattices. Table III displays Fourier coefficients of four particular lattices with two types of motifs. We found that DC provides many equivalent RPL vectors, i.e., many equivalent propagation directions, but the nonlinear coefficients are not always optimum. These nonlinear coefficients vary as a function of lattice but also as a function of motif and propagation direction of the fundamental light beam.

B. Working material and filling factor

It seems that DC is the best structure because of its symmetry and also of the material quantity in a unit cell. Figure 7 illustrates four particular structures, made by spherical motifs. In this illustration, the ratio between radius (R) of motif and QPM structure periodicity (a) is fixed at a reasonable value. The DC structure clearly possesses the largest nonlinear material quantity ($\chi^{(2)} = +1$). As shown in the table of Fig. 7, the best 3D QPM structure should be DC, with highest nonlinear coefficient obtained for the order (1,1,1). However, as mentioned, the nonlinear coefficient depends on the quantity of nonlinear material. In Table III, we can see that the limit of R/a in the DC lattice is $\sqrt{3}/8$. It means that the nonlinear coefficients of the DC structure will be limited by this filling factor. In contrast, it is quite easy to increase the normalized ratio R/a in the case of SC lattice, resulting in higher nonlinear coefficients. We therefore studied the influence of material filling factor on the nonlinear coefficients of a 3D QPM SC structure.

Figures 8 and 9 show the dependence of the nonlinear coefficients of SC lattices on the filling factor (X/a or D/a where $D = 2R$) for cubic and spherical motifs, respectively. Using a SC lattice, the best nonlinear coefficient is obtained by the (1,0,0) QPM order for both kinds of motifs. In the case of square motif maximum efficiency $|\mathbf{G}_{100}|^2 = 0.064$ is obtained for $X/a = 0.73$, while with spherical motif maximum efficiency $|\mathbf{G}_{100}|^2 = 0.101$ is achieved by $D/a = 1$,

SC	
Order	$|G|^2$
(1,0,0)	0.0049
(1,1,0)	0.0033

BCC	
Order	$|G|^2$
(1,1,0)	0.0131
(2,0,0)	0.0053

FCC	
Order	$|G|^2$
(1,1,1)	0.0340
(2,0,0)	0.0241

DC	
Order	$|G|^2$
(1,1,1)	0.0680
(2,2,0)	0.0068
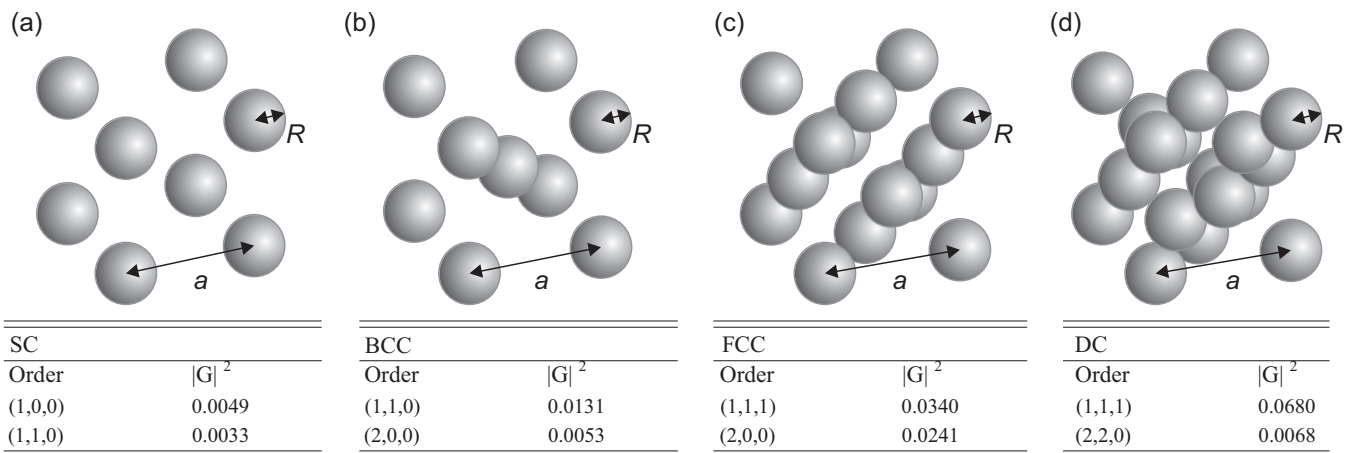
FIG. 7. Four 3D structures with fixed ratio $R/a = \sqrt{3}/8$: (a) SC, (b) BCC, (c) FCC, and (d) DC. The tables present Fourier coefficients of first orders for each corresponding structure. Normalized efficiency is calculated for the "+/–" structure.
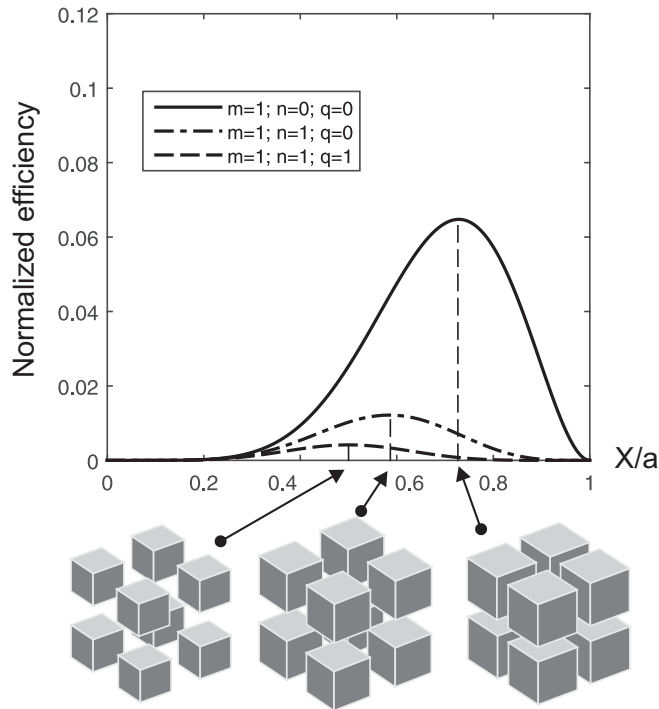
FIG. 8. Normalized efficiency of SC lattice for the three first orders $(1,0,0)$, $(1,1,0)$, and $(1,0,0)$ as a function of ratio between the size of cubic motif, X, and the the lattice periodicity, a. Normalized efficiency is calculated for the "$+/-$" structure.
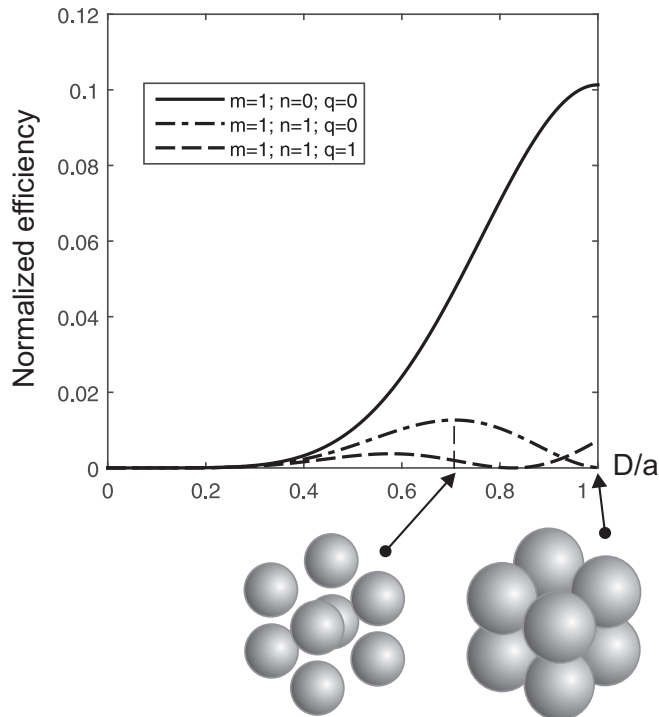
FIG. 9. Normalized efficiency of SC lattice for three first orders $(1,0,0)$, $(1,1,0)$, and $(1,0,0)$ as a function of ratio between the spherical motif diameter, D, and the lattice periodicity, a. Normalized efficiency is calculated for the "$+/-$" structure.

TABLE IV. Optimum Fourier coefficients of SC, BCC, FCC, and DC lattices for "$+/-$" QPM structures, made by two particular motifs.

Order	Cubic motif		Spherical motif	
	$\|\mathbf{G}_{max}\|^2$	X/a	$\|\mathbf{G}_{max}\|^2$	R/a
Simple cubic				
$(1,1,0)$	0.064	0.730	0.101	0.500
$(2,0,0)$	0.012	0.585	0.013	0.353
Body-centered cubic				
$(1,1,0)$	0.041	0.500	0.050	0.352
$(2,0,0)$	0.004	0.365	0.012	0.433
Face-centered cubic				
$(1,1,1)$	0.066	0.500	0.060	0.289
$(2,0,0)$	0.016	0.365	0.025	0.247
Diamond cubic				
$(1,1,1)$	0.016	0.500	0.068	0.216
$(2,2,0)$	0.010	0.500	0.012	0.177

which is higher than the maximum nonlinear coefficient obtained with a DC structure. Again, the spherical motif shows to be the best configuration for 3D QPM structure. We also found that the first QPM order, $(1,0,0)$, is the best direction for 3D QPM, which is also the most efficient process in case of 1D and 2D QPMs, as shown before.

Table IV shows most efficient orders with the highest Fourier coefficients and with corresponding optimum parameters of four lattices. It can be noted that a spherical motif provides better nonlinear coefficients in comparison with those obtained by the cubic motif. This can be explained by the high symmetry of the spherical motif. This result is quite interesting, because the spherical motif is very close to what can be realized in practice. We also found that the SC, the simplest 3D QPM structure, possesses the highest nonlinear coefficient for some particular propagation directions. We suggest that, for nonlinear optics, the QPM could be realized by a simple 3D structure, which reduces challenges of fabrication requirement.

We should note that, in our calculation, the motif possesses a $\chi^{(2)} = +1$, while all surrounding materials possess a $\chi^{(2)} = -1$ or $\chi^{(2)} = 0$. In the case of "$+/-$" QPM structures, we found that there is no difference if the motif possesses an inverse sign, i.e., $\chi^{(2)} = -1$, and the surrounding medium possesses a $\chi^{(2)} = +1$. However, in the case of "$+/0$" or "$0/+$" 3D QPM structures, the results differ. In this case, we defined "block motif" for a situation in which the motif possesses $\chi^{(2)} = +1$ and the surrounding medium possesses $\chi^{(2)} = 0$ and a "hollow motif" for the situation in which the motif possesses $\chi^{(2)} = 0$ and the surrounding medium possesses $\chi^{(2)} = +1$. Using linearity of a Fourier transform, we can calculate the nonlinear efficiency of SC structures made by hollow and block motifs. Figure 10 shows the variation of the nonlinear coefficients as a function of filling factor (volume of nonlinear material divided by volume of unit cell) for the block motif (solid line) and for the hollow motif (dashed line). When $V_{\text{nonlinear material}}/V_{\text{unit cell}}$ is zero, there is no active material and the QPM effect is canceled. When $V_{\text{nonlinear material}}/V_{\text{unit cell}}$ is equal to 1, we have only active material and the same situation occurs. A crossing of curves is obtained when the motif size is equal to a half of length of unit cell. The insert of Fig. 10 shows the evolution
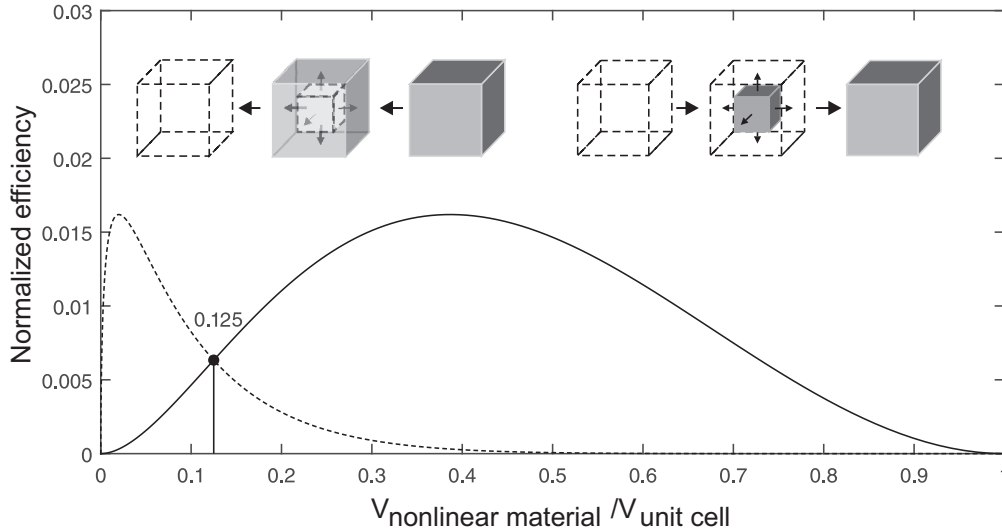
FIG. 10. Normalized efficiency for (1,0,0) order of a SC lattice with a cubic motif. The solid and dashed lines represent efficiency curves of 3D QPM structures made by solid and inverse (hollow) motifs, respectively. The insert shows the evolution from full material to null material (hollow motif) and from null to full material (block motif).

from full material to null material (hollow motif) and from null to full material (block motif).

C. Real structure approach

In reality, motifs are more complicated, depending on the fabrication technologies and materials used. 3D QPM structures could be only fabricated by optical lithographies techniques on polymer materials. For example, a 3D template with $\chi^{(2)} = 0$ can be fabricated by an interference technique [34], which is simple and useful for the fabrication of large-area, uniform, and controllable forms. The third dimension of these 3D structures can be as thick as desired by using a holographic assembly technique [40] or as thick as 300 μm by using an ultra-low absorption method [41]. The fabricated structures can be then filled by a nonlinear material [$\chi^{(2)} = +1$], resulting in a "+/0" QPM 3D structure. Note that the polymeric structure [$\chi^{(2)} = 0$] and the nonlinear material [$\chi^{(2)} \neq 0$] have the same refractive indices. Therefore, there is no lost of the fundamental and harmonic lights due to the scattering or diffraction effect. The 3D structures fabricated by this method consist of main motifs (spherelike) connected to each other by nanoconnections in form of a grid. We therefore performed the calculation of nonlinear conversion efficiency by taking into account this "real structure approach." In this section, we present the results obtained with SC lattices with two types of connections: "square-cut" and "circular-cut," but only the last one is presented in Fig. 11.

For calculations we introduced a spherical motif [$\chi^{(2)} = +1$] with a radius R in the center of the SC lattice unit cell. The unit cell is repeated by a period of a in x, y, and z directions. Each spherical motif has six symmetrical circular-cut connections [$\chi^{(2)} = +1$], where the cross section has a radius of r [Fig. 11(a)]. Using the property of linearity of the Fourier transform, we calculate the Fourier coefficients for these two complicated motifs, as shown in Table V. It should be mentioned that the connections are rather small in comparison with the main motif and that this

assumption allows us to simplify the form of connection as orthorhombic ("square-cut") and cylindrical ("circular-cut") forms.

Figure 11(b) represents the surface of normalized efficiency for a SC QPM structure ("+/0" type) made by spherical motifs with cylindrical nanoconnections. Normalized efficiency was calculated for optimum (1,0,0) order. In the case of $r/a = 0$, we got a result similar to the case of a simple spherical motif (without connection). Also, it should be noted that the normalized radius of spherical motif has lower limit $R/a > r/a$ because the size of connections should not exceed the size of the main motif. We found a slight increase of the nonlinear coefficient as a function of the r/a parameter. This is explained by the increase of the quantity of nonlinear material. However, considering a limitation of cylindrical connections as $r/a \leqslant 0.1$, the increase is very modest, as shown in Fig. 11(b). It means that nanoconnections have a slight influence on normalized efficiency and could be neglected in the calculation of more complicated structures.
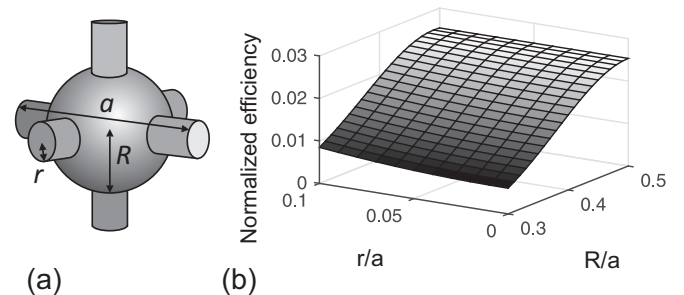
FIG. 11. (a) Spherical motifs with "circular-cut" connections. a is lattice period, R is radius of sphere located in the center of unit cell, and r is radius of circular cut. (b) Surface of normalized efficiency of corresponding 3D QPM structure as a function of $r/a \leqslant 0.1$ and $0.3 \leqslant R/a \leqslant 0.5$. Normalized efficiency is calculated for (1,0,0) order for "+/0" QPM structure.

TABLE V. Fourier coefficients for two types of 3D "+/0" QPM structures: Spherical motif with square-cut connections and with circular-cut connections.

Motif	Fourier coefficients
Spherical motif with square-cut connections	$H = 2\pi\sqrt{m^2 + n^2 + q^2}$ $\mathbf{G}_{mnq} = \frac{4\pi}{H^3}[\sin{(H\frac{R}{a})} - H\frac{R}{a}\cos{(H\frac{R}{a})}] + \frac{L^2}{a^2}\mathrm{sinc}(n\frac{L}{a})\mathrm{sinc}(q\frac{L}{a})[\mathrm{sinc}(m) - 2\frac{R}{a}\mathrm{sinc}(2m\frac{R}{a})]$ $\qquad + \frac{L^2}{a^2}\mathrm{sinc}(m\frac{L}{a})\mathrm{sinc}(q\frac{L}{a})[\mathrm{sinc}(n) - 2\frac{R}{a}\mathrm{sinc}(2n\frac{R}{a})]$ $\qquad + \frac{L^2}{a^2}\mathrm{sinc}(m\frac{L}{a})\mathrm{sinc}(n\frac{L}{a})[\mathrm{sinc}(q) - 2\frac{R}{a}\mathrm{sinc}(2q\frac{R}{a})]$
Spherical motif with circular-cut connections	$H = 2\pi\sqrt{m^2 + n^2 + q^2}$ $\mathbf{G}_{mnq} = \frac{4\pi}{H^3}[\sin{(H\frac{R}{a})} - H\frac{R}{a}\cos{(H\frac{R}{a})}] + \frac{r}{a}\frac{1}{\sqrt{n^2+q^2}}J_1(2\pi\frac{r}{a}\sqrt{n^2+q^2})[\mathrm{sinc}(m) - 2\frac{R}{a}\mathrm{sinc}(2m\frac{R}{a})]$ $\qquad + \frac{r}{a}\frac{1}{\sqrt{m^2+q^2}}J_1(2\pi\frac{r}{a}\sqrt{m^2+q^2})[\mathrm{sinc}(n) - 2\frac{R}{a}\mathrm{sinc}(2n\frac{R}{a})]$ $\qquad + \frac{r}{a}\frac{1}{\sqrt{m^2+n^2}}J_1(2\pi\frac{r}{a}\sqrt{m^2+n^2})[\mathrm{sinc}(q) - 2\frac{R}{a}\mathrm{sinc}(2q\frac{R}{a})]$ In particular case $\sqrt{n^2 + q^2} = 0$: $\frac{r}{a}\frac{1}{\sqrt{n^2+q^2}}J_1(2\pi\frac{r}{a}\sqrt{n^2+q^2}) = \pi\frac{r^2}{a^2}$

V. CONCLUSION

In this paper, we have presented a general analysis of quasi-phase-matched conversion efficiency in periodic 3D structures. We investigated in detail the nonlinear conversion efficiency of 3D QPM structures with different choices of lattice, shape, and dimensions of the nonlinear motif. General data displayed in Table II and Table III can be used to calculate Fourier coefficients of any QPM order. We demonstrated that this general theory is applicable to 1D and 2D QPM structures, as reported in previous papers. It shows that the conversion efficiency of the 3D QPM structures is weaker than that of the 2D QPM and the later one is also weaker than that of the 1D QPM. It is explained by the quantity of the nonlinear material in each motif of a QPM structure and in good logic and proportion. However, the 3D QPM structure possesses much more QPM orders than 1D and 2D structures, and hence it enhances the flexibility of the RLV design and enables more complicated nonlinear processes in the same 3D structure.

Furthermore, we have investigated the optimization of the 3D structure's configuration to achieve the best nonlinear conversion efficiency. Four possible structures are studied, SC, BCC, FCC, and DC lattices with square and spherical motifs, showing high conversion efficiency. The filling factor of those structures was also optimized to obtain optimum conversion efficiency. Simple cubic 3D structure is a very simple structure but it is the most efficient 3D QPM structure. Normalized efficiency plots of SC lattice for cubic and spherical motifs revealed strong influence of filling factor on conversion efficiency of a nonlinear process.

Finally, we have drawn a lot of attention to connection of our theoretical work with real structures. We made an accent on structures, which can be fabricated in practice by a simple method, such as interference lithography. Description and analysis of theoretical structures with small connections between motifs, which are very close to real structures, were stated. We demonstrated that, due to the small quantity of nonlinear material of the connection, it has a slight influence on normalized nonlinear conversion efficiency and, theoretically, could be neglected.

[1] J. A. Giordmaine, Phys. Rev. Lett. **8**, 19 (1962).

[2] P. D. Maker, R. W. Terhune, M. Nisenoff, and C. M. Savage, Phys. Rev. Lett. **8**, 21 (1962).

[3] R. Danielius, A. Piskarskas, P. Di Trapani, A. Andreoni, C. Solcia, and P. Foggi, Opt. Lett. **21**, 973 (1996).

[4] D. J. Armstrong, W. J. Alford, T. D. Raymond, A. V. Smith, and M. S. Bowers, J. Opt. Soc. Am. B **14**, 460 (1997).

[5] A. V. Smith, D. J. Armstrong, and W. J. Alford, J. Opt. Soc. Am. B **15**, 122 (1998).

[6] J. A. Armstrong, N. Bloembergen, J. Ducuing, and P. S. Pershan, Phys. Rev. **127**, 1918 (1962).

[7] P. A. Franken and J. F. Ward, Rev. Mod. Phys. **35**, 23 (1963).

[8] M. M. Fejer, G. A. Magel, D. H. Jundt, and R. L. Byer, IEEE J. Quant. Electron. **28**, 2631 (1992).

[9] V. Berger, Phys. Rev. Lett. **81**, 4136 (1998).

[10] N. G. R. Broderick, G. W. Ross, H. L. Offerhaus, D. J. Richardson, and D. C. Hanna, Phys. Rev. Lett. **84**, 4345 (2000).

[11] A. Chowdhury, C. Staus, B. F. Boland, T. F. Kuech, and L. McCaughan, Opt. Lett. **26**, 1353 (2001).

[12] N. G. R. Broderick, R. T. Bratfalean, T. M. Monro, D. J. Richardson, and C. M. de Sterke, J. Opt. Soc. Am. B **19**, 2263 (2002).

[13] S. Saltiel and Y. S. Kivshar, Opt. Lett. **25**, 1204 (2000).

[14] S. M. Saltiel and Y. S. Kivshar, Opt. Lett. **27**, 921 (2002).

[15] K. L. Vodopyanov, O. Levi, P. S. Kuo, T. J. Pinguet, J. S. Harris, M. M. Fejer, B. Gerard, L. Becouarn, and E. Lallier, Opt. Lett. **29**, 1912 (2004).

[16] G. Imeshev, A. Galvanauskas, D. Harter, M. A. Arbore, M. Proctor, and M. M. Fejer, Opt. Lett. **23**, 864 (1998).

[17] T. Ellenbogen, N. Voloch-Bloch, A. Ganany-Padowicz, and A. Arie, Nat. Photon. **3**, 395 (2009).

[18] A. Shapira, R. Shiloh, I. Juwiler, and A. Arie, Opt. Lett. **37**, 2136 (2012).

[19] J. Chen and X. Chen, Phys. Rev. A **80**, 013801 (2009).

[20] J. Chen and X. Chen, J. Opt. Soc. Am. B **28**, 241 (2011).

[21] S. Stivala, F. Buccheri, L. Curcio, R. L. Oliveri, A. C. Busacca, and G. Assanto, Appl. Phys. Lett. **62**, 435 (1993).

[22] T. Xu, D. Lu, H. Yu, H. Zhang, Y. Zhang, and J. Wang, Appl. Phys. Lett. **108**, 051907 (2016).

[23] L. A. Eyres, P. J. Tourreau, T. J. Pinguet, C. B. Ebert, J. S. Harris, M. M. Fejer, L. Becouarn, B. Gerard, and E. Lallier, Appl. Phys. Lett. **79**, 904 (2001).

[24] V. Taggi, F. Michelotti, M. Bertolotti, G. Petrocco, V. Foglietti, A. Donval, E. Toussaere, and J. Zyss, Appl. Phys. Lett. **72**, 2794 (1998).

[25] S. Yilmaz, S. Bauer, and R. Gerhard-Multhaupt, Appl. Phys. Lett. **64**, 2770 (1994).

[26] A. Apostoluk, D. Chapron, G. Gadret, B. Sahraoui, J. M. Nunzi, C. Fiorini-Debuisschert, and P. Raimond, Opt. Lett. **27**, 2028 (2002).

[27] G. Martin, S. Ducci, R. Hierle, D. Josse, and J. Zyss, Appl. Phys. Lett. **83**, 1086 (2003).

[28] G. L. J. A. Rikken, C. J. E. Seppen, S. Nijhuis, and E. W. Meijer, Appl. Phys. Lett. **58**, 435 (1991).

[29] O. Sugihara, M. Nakanishi, Y. Che, C. Egami, Y. Kawata, and N. Okamoto, App. Opt. **39**, 5632 (2000).

[30] X. Ni, M. Nakanishi, O. Sugihara, and N. Okamoto, Opt. Rev. **5**, 9 (1998).

[31] J. H. Lin, N. D. Lai, C. H. Chiu, C. Y. Lin, G. W. Rieger, J. F. Young, F. S. S. Chienc, and C. C. Hsua, Opt. Express **16**, 7832 (2008).

[32] M. Farsari, A. Ovsianikov, M. Vamvakaki, I. Sakellari, D. Gray, B. N. Chichkov, and C. Fotakis, Appl. Phys. A **93**, 11 (2008).

[33] D. B. Do, J. H. Lin, N. D. Lai, H. C. Kan, and C. C. Hsu, Appl. Opt. **50**, 4664 (2011).

[34] N. D. Lai, W. P. Liang, J. H. Lin, C. C. Hsu, and C. H. Lin, Opt. Express **13**, 9605 (2005).

[35] S. M. Russel, P. E. Powers, M. J. Missey, and K. L. Scheple, IEEE J. Quant. Electron. **37**, 877 (2001).

[36] A. Arie and N. Voloch, Laser & Photon. Rev. **4**, 355 (2010).

[37] C. Kittel, *Introduction to Solid State Physics*, 7th ed. (Wiley, New York, 1995).

[38] A. Arie, N. Habshoosh, and A. Bahabad, Opt. Quant. Electron. **39**, 361 (2007).

[39] K. M. Ho, C. T. Chan, and C. M. Soukoulis, Phys. Rev. Lett. **65**, 3152 (1990).

[40] N. D. Lai, D. B. Do, J. H. Lin, and C. C. Hsu, Appl. Phys. A **100**, 171 (2010).

[41] Q. Li, M. T. Do, I. Ledoux-Rak, and N. D. Lai, Opt. Lett. **38**, 4640 (2013).